

Tree crown segmentation in three dimensions using density models derived from airborne laser scanning

Johan Holmgren, Eva Lindberg, Kenneth Olofsson & Henrik J. Persson

To cite this article: Johan Holmgren, Eva Lindberg, Kenneth Olofsson & Henrik J. Persson (2022) Tree crown segmentation in three dimensions using density models derived from airborne laser scanning, International Journal of Remote Sensing, 43:1, 299-329, DOI: [10.1080/01431161.2021.2018149](https://doi.org/10.1080/01431161.2021.2018149)

To link to this article: <https://doi.org/10.1080/01431161.2021.2018149>



© 2022 The Author(s). Published by Informa UK Limited, trading as Taylor & Francis Group.



Published online: 05 Jan 2022.



Submit your article to this journal [↗](#)



Article views: 179




View related articles [↗](#)



View Crossmark data [↗](#)

Tree crown segmentation in three dimensions using density models derived from airborne laser scanning

Johan Holmgren , Eva Lindberg , Kenneth Olofsson  and Henrik J. Persson 

Department Forest Resource Management, Swedish University of Agricultural Sciences, Umeå, Sweden

ABSTRACT

This article describes algorithms to extract tree crowns using two-dimensional (2D) and three-dimensional (3D) segmentation. As a first step, a 2D-search detected the tallest trees but was unable to detect trees located below other trees. However, a 3D-search for local maxima of model fits could be used in a second step to detect trees also in lower canopy layers. We compared tree detection results from ALS carried out at 1450 m above ground level (high altitude) and tree detection results from ALS carried out at 150 m above ground level (low altitude). For validation, we used manual measurements of trees in ten large field plots, each with an 80 m diameter, in a hemiboreal forest in Sweden (lat. 58°28' N, long. 13° 38' E). In order to measure the effect of using algorithms with different computational costs, we validated the tree detection from the 2D segmentation step and compared the results with the 2D segmentation followed by 3D segmentation of the ALS point cloud. When applying 2D segmentation only, the algorithm detected 87% of the trees measured in the field using high-altitude ALS data; the detection rate increased to 91% using low-altitude ALS data. However, when applying 3D segmentation as well, the algorithm detected 92% of the trees measured in the field using high-altitude ALS data; the detection rate increased to 99% using low-altitude ALS data. For all combinations of algorithms and data resolutions, undetected trees accounted for, on average, 0–5% of the total stem volume in the field plots. The 3D tree crown segmentation, which was using crown density models, made it possible to detect a large percentage of trees in multi-layered forests, compared with using only a 2D segmentation method.

ARTICLE HISTORY

Received 31 May 2021

Accepted 1 December 2021

1. Introduction

Information about individual trees can now be derived using algorithms that delineate tree crowns in Airborne Laser Scanning (ALS) data (Hyypä et al. 2008). Decision makers can use such tree maps to monitor forests for environmental and climate changes, and optimize the utilization of natural resources to achieve multiple goals such as the supply of bio-based products and biodiversity. Tree level information is the basis for a new type of forestry – precision forestry (Holopainen, Vastaranta and Hyypä 2014).

CONTACT Johan Holmgren  Johan.Holmgren@slu.se  Department Forest Resource Management, Swedish University of Agricultural Sciences, Umeå, Sweden

© 2022 The Author(s). Published by Informa UK Limited, trading as Taylor & Francis Group.

This is an Open Access article distributed under the terms of the Creative Commons Attribution-NonCommercial-NoDerivatives License (<http://creativecommons.org/licenses/by-nc-nd/4.0/>), which permits non-commercial re-use, distribution, and reproduction in any medium, provided the original work is properly cited, and is not altered, transformed, or built upon in any way.

ALS data with low resolution are already available for large forested areas, and have been used for operational surveys, such as the recently implemented national forest mapping projects (Nilsson et al. 2017). On the other hand, ALS data with sufficient resolution to detect individual trees have not been feasible for the mapping of large forest areas in the past, because of a high cost per area unit for large areas, and due to high set-up costs for small areas. However, the potential to cover large areas has recently improved. Two main system categories can now provide ALS data with a resolution high enough to detect individual trees: (1) large-area survey ALS systems that provide high-resolution (>10 pulses m^{-2}) data from high altitudes (Swatantran et al. 2016), and (2) short-range systems operated from helicopters or drones, providing ultra-high-resolution (>100 pulses m^{-2}) for specific areas of interest and with a lower set-up cost (Kellner et al. 2019). All of these ALS systems enable efficient mapping of forests and produce large amounts of data. Therefore, algorithms for extraction of individual tree information should both be computationally efficient and be able to adapt to the different site conditions that may occur across large geographical areas.

Challenges in delineating individual tree crowns from ALS data relate to the physical principles of laser scanning. Laser systems emit laser pulses and digitize the amplitude of the returned signals at discrete time intervals. The system saves the waveform described by the amplitude data for the returned signal and/or local maxima of the returned signal (i.e. returned pulses). The system typically records single return pulses only if a solid surface is measured (such as flat ground without vegetation) but, when forested areas are being measured, more often multiple pulses are returned (Baltsavias 1999). Hence, ALS detects non-solid as well as solid surfaces in forests, making it difficult to distinguish trees using surface-model-based algorithms that detect tree crown boundaries.

A common approach used for many tree detection algorithms is first to create a digital surface model (DSM), which is a two-dimensional (2D) raster with height (i.e. distance to ground) assigned to raster cell values, then to estimate tree locations from local maxima within the DSM. The final step is to delineate tree crowns using a watershed segmentation (Lindberg and Holmgren 2017). This approach suffers from at least two major problems. The first problem is caused by the non-solid properties of tree crowns. Laser pulse returns are usually located somewhere inside tree crowns and not just at the top of the canopy, which is the assumption made when tree crown delineation algorithms find local maxima of a DSM. Therefore, researchers have developed algorithms that find the outermost parts of the canopy, for example, using active contours (Persson, Holmgren and Söderman 2002). However, smaller trees close to taller trees may be located below such a surface, and so detection of trees will depend on the parameter settings for the algorithm used to construct the surface. The second issue arising from using algorithms with a DSM is how to select the scale parameters, which usually includes one affecting the smoothing of the DSM. The tree detection results will depend on a combination of tree size, tree crown shape at a given place, and scale parameters. Some previous studies have addressed this scale problem by using multiscale approaches and variable window sizes determined from empirical relationships (Persson, Holmgren and Söderman 2002; Popescu, Wynne and Nelson 2002; Wolf and Heipke 2007; Bian et al. 2014; Falkowski et al. 2006).

The surface-based algorithms guarantee robustness and computational efficiency but, since the algorithms exclude sub-canopy data, they are only suitable for certain applications. However, the algorithms can often estimate forest volume and biomass with sufficient accuracy, since the tallest, dominant trees contribute the greatest to these variables.

However, mapping of the understory requires algorithms that utilize laser data in other ways. Methods for three-dimensional (3D) segmentation, hence trying to overcome the previously described challenges, still often use surface-based approaches as a first step and then use information from the first step when analyzing the whole point cloud (Kandare et al. 2016; Wu et al. 2013; Bucksch et al. 2013; Lu et al. 2014.). Some algorithms include k-means clustering (Morsdorf et al. 2003; Gupta, Weinacker and Koch 2010; Lindberg et al. 2014), stem detection (Mongus and Žalik 2015), and normalized cuts (Reitberger et al. 2009). There are also approaches that use region growing (Lee et al. 2010; Vaughn, Moskal and Turnblom 2012; Wang et al. 2016).

In this article, we describe two segmentation algorithms (2D and 3D segmentation), both using templates (i.e. model of the tree crown density) derived from empirical data. The 2D segmentation algorithm creates a model fit surface rather than a traditional surface model of the canopy. The templates are based on the discrete probability density function of laser returns from different locations in tree crowns (i.e. density models). The 2D segmentation algorithm is a refinement of an earlier algorithm (Holmgren and Lindberg 2019) which, in turn, was an improvement of an algorithm based on solid geometric tree crown templates (Holmgren and Lindberg 2013). Our work described in this article further improves this 2D algorithm through another function to derive the model fit surface, repeated use of watershed segmentation. The new 3D segmentation algorithm uses the output from the 2D segmentation, and further separates trees located below other trees. The 3D segmentation algorithm uses clustering of 3D points based on model fit strings derived using tree crown templates (i.e. density models). For both algorithms, instead of attempting to overcome the problem of noise caused by laser returns inside tree crowns, we included these laser returns as part of a density model of the tree crowns. To address the challenge of finding optimal scale parameters, we used templates derived from crown density models trained with empirical data. We validated the algorithms using high-altitude ALS data to understand the feasibility of applying the algorithms to large-area mapping. We also validated the algorithms using ultra-high-resolution data from low-altitude ALS to understand whether it was data resolution or the algorithms themselves that limited the obtained tree detection accuracy. The objectives were: (1) to validate algorithms based on crown density models, (2) to compare 2D and 3D segmentation, and (3) to compare tree detection using ALS data from low and high altitudes.

2. Material

2.1. Study area

The segmentation method was validated using manually measured tree positions in ten circular field plots, each with 80 m diameter, located at the test site at Remningstorp (lat. 58° 28' N, long. 13°38' E) in southern Sweden. The test site mainly contains managed hemiboreal forest dominated by Norway spruce (*Picea abies*) and Scots pine (*Pinus sylvestris*), but also includes deciduous trees, mostly Birch (*Betula sp.*) and Oak (*Quercus robur*).

2.2. Airborne laser scanning

To obtain data that were suitable for large-area mapping, the airborne laser scanner (ALS) system Leica Terrain Mapper was operated between 1422 m and 1450 m above ground level, at a flight speed of 278 km h⁻¹. The test site was laser scanned in October 2019. The field of view was 30 degrees with an elliptical scan pattern. The elliptical scan pattern, combined with sidewise overlap between flight strips, resulted in laser measurements of trees from up to four directions. The pulse repetition frequency was 1600 kHz. The scanner frequency was 150 Hz. The laser footprint was .35 m. The nominal density of last or single returns as derived from the mission plan was approximately 22 points m⁻². The observed ALS density was, on average, 69 returns m⁻² in the field plots used for validation, including buffer zones.

To obtain high-resolution data to study the limitations of the algorithms, the airborne laser scanner system Riegl MLS-Q680i was operated from a helicopter at a flight altitude of 150 m above ground level. The field plots used in this study were laser scanned in December 2018. Each field plot was covered with multiple flyovers from different directions to obtain high-resolution ALS data. The laser scanner was mounted with the scanner level approximately 15 degrees to the forward direction which, in combination with multiple flyovers of the field plots, resulted in multiple views of tree crowns from the side. The observed ALS density was, on average, 2511 returns m⁻² in the field plots used for validation, including buffer zones.

For both datasets, the laser returns were classified as ground and non-ground returns using the software TerraScan from Terrasolid. We replaced the original z values of the laser returns with height above the ground (z) using the same software. We used the height-normalized ALS data (x, y, z) as input to the tree crown segmentation algorithms.

2.3. Field data

A manual field inventory of ten 80 m diameter field plots was carried out in May 2019. As instructed, the stem diameters (DBH) of all trees with ≥ 4 cm stem diameter at 1.3 m above ground level were measured in two directions using a calliper. The eight of the sample trees was measured with a hypsometer. In each plot, 16 subplots were systematically distributed to facilitate measurement of tree positions. Tree positions were measured in the subplots using ultrasonic trilateration (POSTEX, Haglöf Sweden AB) with a maximum working range of approximately 15 m from the subplot center. The POSTEX equipment was integrated with a digital calliper with tree positions measured relative to the subplot center. Approximate positions of each subplot center were measured using a Global Navigation Satellite System (GNSS) and were used as starting positions for a co-registration algorithm. The field plot co-registration carried out in this study used a previously developed algorithm (Olofsson, Lindberg and Holmgren 2008). The technique is based on synthetic tree position images where the coordinates determine the position within the image and the size variable, for instance the stem diameter, determines the amplitude of a Gaussian function. The field plot image can be rotated a few degrees between each correlation run, to compensate for possible compass errors. The position with the highest normalized correlation coefficient was considered a possible position of the field plot within the coordinate system of the forest area. Tree coordinates of the subplots can be transformed to global coordinates using the described co-registration algorithm, even when the accuracy of the subplot center position measurement is

Table 1. Summary of the field data used for validation.

Plot	Stem density (numberha ⁻¹)	DBH Average (mm)	DBH Min (mm)	DBH Max (mm)	Proportion Pine (%)	Proportion Spruce (%)	Proportion Deciduous (%)
1	613	297	49	469	0	97	3
2	420	258	50	397	2	84	14
3	643	298	47	514	0	93	7
4	462	258	86	405	0	97	3
5	348	287	175	435	14	86	0
6	523	282	43	498	52	48	0
7	643	172	42	465	31	62	7
8	485	281	55	421	0	82	18
9	352	314	42	507	84	3	14
10	436	301	72	509	0	94	6

poor. Thus, tree coordinates from all subplots could be merged to a large circular field plot of 80 m diameter. The tree coordinates of the large field plot were then matched a second time with the tree map from ALS data to improve the transformation to global coordinates further. The heights (H) of field-measured trees (except sample trees) were estimated using regression functions as described in Persson and Fransson (2017). For the estimations, separate functions were used for different tree classes (Scots pine, Norway spruce, and deciduous trees) using DBH as the explanatory variable for all tree classes, and also using plot-level basal area for Scots pine and Norway spruce. The parameters of the functions were estimated using a large database consisting of sample trees from several field inventories at the test site. The stem volumes of field-measured trees were derived using volume functions for southern Sweden (Brandel 1990), with H and DBH as input variables. A summary of the field inventory data for the plots used for validation is presented in Table 1.

3. Methods

The segmentation algorithms used tree crown templates, each consisting of a 2D density raster with cells representing density of the 3D space in washer-shaped slices ('washers') extracted from tree crowns. For the density raster, one dimension is relative distance from ground and the other dimension is relative distance from tree centre. The relative distance was calculated by dividing distance by tree height (i.e. raster cell value of a canopy height model). The segmentation algorithms derived templates in a training phase, using ALS data inside manually delineated tree crown polygons. For the prediction phase, the templates were fitted to ALS data at raster cell locations within the laser-scanned area. A model fit (MF) surface was created by deriving a model coefficient with values between zero and one, with a value of one for a perfect fit. The MF surface was then used for 2D segmentation, followed by a 3D segmentation using MF strings. In the following subsections, we describe the entire segmentation procedure in detail. Overviews of the algorithms are shown in Figure 1 and Table 2.

3.1. Tree crown template

3.1.1. Tree crown density model

A tree crown template is a density model (i.e. a raster describing tree crown density) based on ALS data from the vegetation (i.e. ALS returns above a height threshold). The template can be created using ALS data in manually delineated tree crown polygons. In the training phase, the

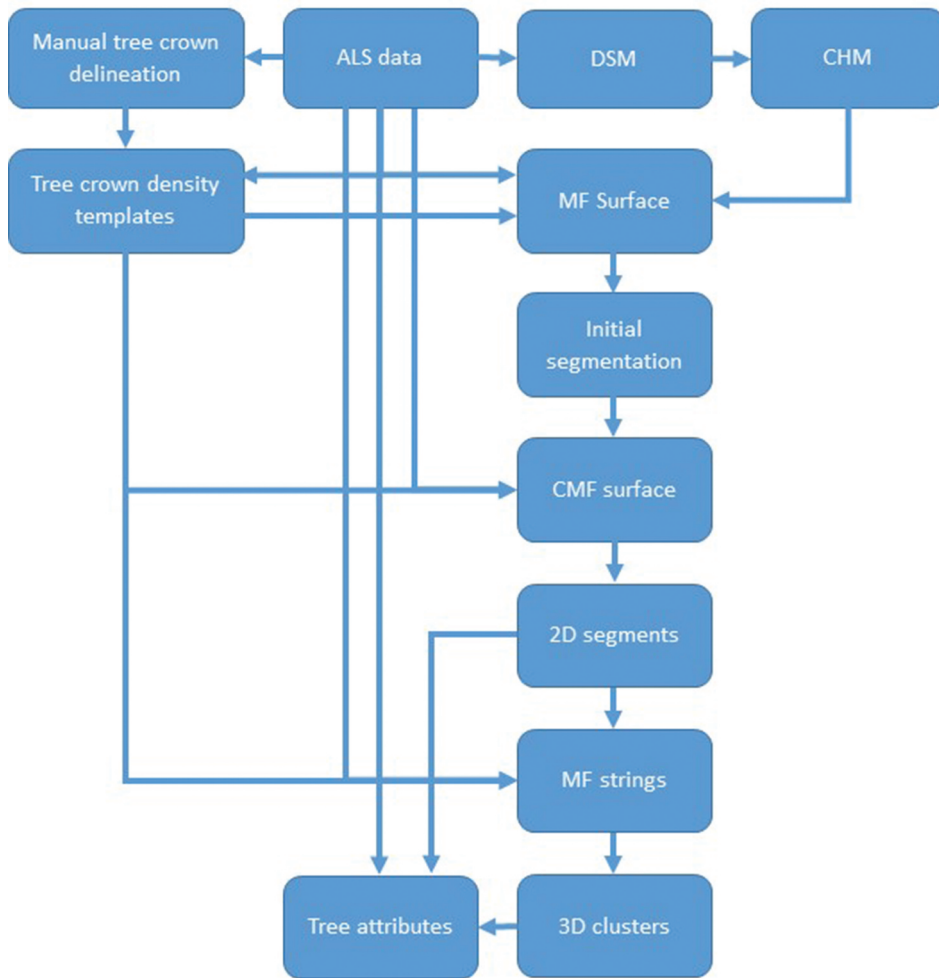


Figure 1. Overview of the segmentation algorithms using templates (i.e. tree crown density models).

model centre (x_c, y_c) was defined as the mean value of x and y coordinates of all laser returns above a height threshold within the manually delineated tree crown polygon. The model includes a tree height (h_{\max}) which, for the training phase, was set as the maximum height of laser returns located within the manually delineated tree crown. From the model centre, laser returns were selected within a search radius and each laser return was projected onto a height-radius plane to create a tree crown density raster (Figure 2). The raster cell values were derived using accumulated values of projected laser returns. This was carried out as follows: for each laser return above a height threshold, the distance r to the tree crown centre was calculated using Equation 1. This distance and the height of the laser return were used to calculate a relative radial distance r_p to the tree centre (Equation 2) and relative height h_p (Equation 3) by dividing with the maximum height above the ground (h_{\max}) . The raster indices were calculated by dividing the radial distance with the raster cell size m (set to .01, proportion of h_{\max}), where index i represents the radius dimension (Equation 4) and index j represents the height

Table 2. Algorithm summary.

Input	Unit	Action	Output
Files with ALS data of manually delineated trees crowns ALS data	Do for ALS data from each tree crown in the training dataset Do for each raster cell within the laser-scanned area	For the associated crown density raster: loop the raster and aggregate laser return values to raster cells Set raster cell value to the height value of the laser return contained in the raster cell with the maximum distance from ground	Templates DSM
DSM	Do for each raster cell of the laser-scanned area	Set raster cell value to one if the maximum height (DSM) is above a height threshold (2 m) followed by morphological closing	Canopy area raster
DSM; canopy area raster	Do for each raster cell within the laser-scanned area	Set raster cell value to the DSM. If the value of the DSM is zero but the canopy area raster is one, interpolate a height using the smallest window needed to find a neighboring raster cell with canopy DSM values above zero	Canopy Height Model (CHM)
CHM; ALS data; templates (one for each tree class)	Do for each raster cell within the laser-scanned area	Derive a tree crown model using surrounding data and calculate B value, one for each of the templates, and save the maximum B value in the raster cell	Model Fit Surface (MFS)
MFS	Do for each raster cell within the laser-scanned area	Calculate a new value of the model fit surface using a Gaussian kernel, which produces a smoothed model fit surface	Smoothed MFS
Smoothed MFS	Do for each raster cell within the laser-scanned area	Watershed segmentation: starting at each raster cell, create a path by traveling to a neighboring raster cell in the steepest direction	Initial segmentation
CHM; ALS data; templates; Initial segmentation	Do for each raster cell within the laser-scanned area	Derive a tree crown model using surrounding data only from locations within the same segment, and calculate B value, one for each of the templates, and save the maximum B value in the raster cell	CMF Surface
CMF Surface	Do for each raster cell of the laser-scanned area	Derive a model fit surface using a Gaussian kernel	Smoothed CMF surface
Smoothed CMF surface	Do for each raster cell within the laser-scanned area	Watershed segmentation: starting at this raster cell, create a path by traveling to a neighboring raster cell in the steepest direction	Final 2D segmentation
Final 2D segmentation; ALS data	Do for each crown segment within the laser-scanned area	Find the tree center position, tree height, crown area, and other variables derived from laser data within a crown segment	File with tree attributes
ALS data; Final 2D segment	Do for each crown segment within the laser-scanned area	Derive 3D points with model fit coefficient	MF strings
MF strings	Do for each 3D point of the model fit strings within each 2D segment	Find cluster centres using the mean shift algorithm	3D points with cluster identification

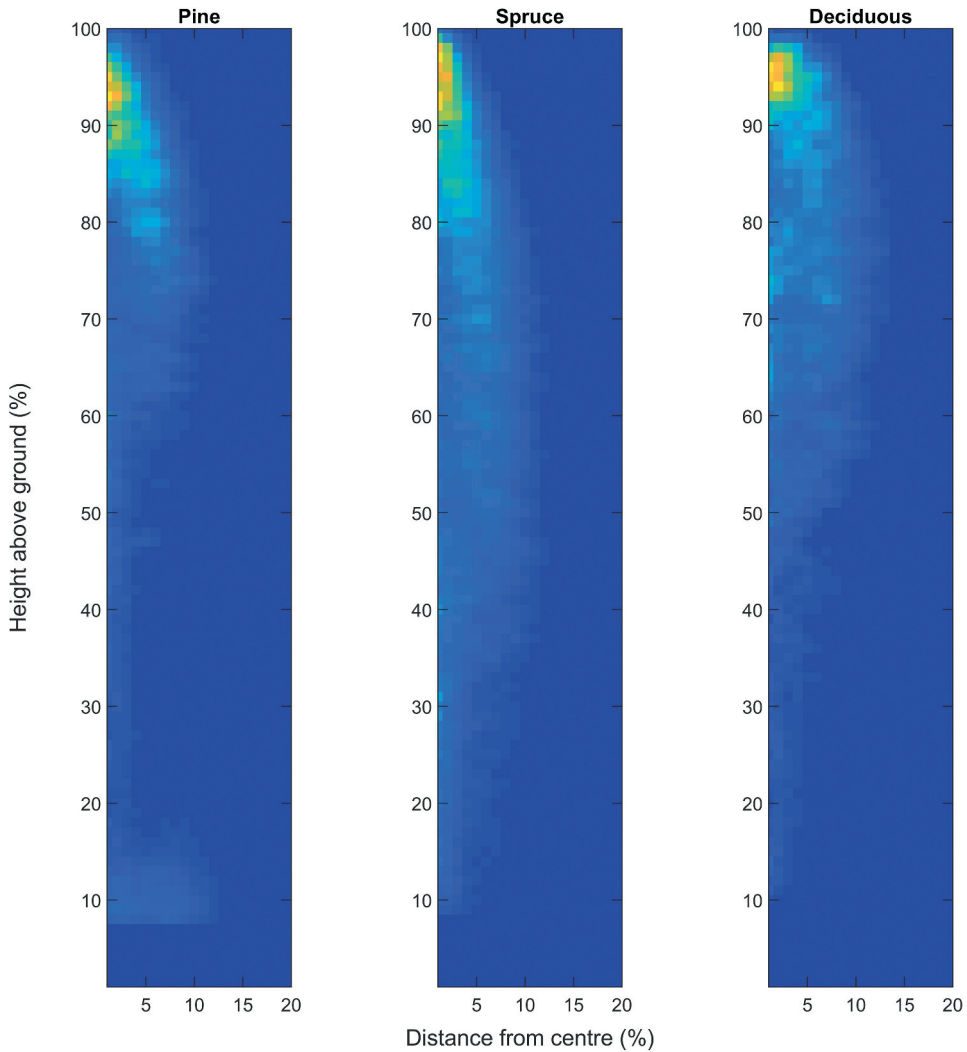


Figure 2. The templates created in the training phase using low-altitude ALS data.

dimension (Equation 5) of the 2D crown density raster. For a density raster that represented the model for a specific tree class, the value a divided by the volume that the raster cell represented (Equation 6) was accumulated; this was repeated for all laser returns within the washer ($k = 1 \dots n$). In this work, the value a was set to one, but could also be an attributed value of a laser return describing crown density, such as amplitude of the returned laser signal. The Δr_i is the horizontal width of the washer and Δh_j is the vertical width of the washer.

$$r = \sqrt{(x - x_c)^2 + (y - y_c)^2} \quad (1)$$

$$r_p = r/h_{max} \quad (2)$$

$$h_p = h/h_{max} \quad (3)$$

$$i = r_p/m \quad (4)$$

$$j = h_p/m \quad (5)$$

$$d_{ij} = \sum_{k=1}^n a/(r_i^2\pi - (r_i - \Delta r_i)^2\pi)\Delta h_j \quad (6)$$

3.1.2. Create tree crown templates with empirical data

The laser scanning data used for training were selected by manual delineation of individual tree crowns. In this work, we used three different tree classes: Scots pine, Norway spruce, and deciduous trees. We used visualizations of high-resolution ALS data to delineate polygons, which were used to extract ALS data for individual tree crowns. The laser data within the tree crowns from a tree class were then scaled, combined into one, and projected onto the height-radius plane, as given by the crown density model (Equations 1–6). For the training phase, h_{max} was the maximum height above the ground (z) of all laser returns in the tree crown polygon given by the manual delineation. The use of the projection to the height-radius plane means that the matching procedure assumes rotational symmetry around the tree center. These crown density models are more robust compared to algorithms based only on canopy height surface models, since laser returns within a tree crown no longer appear as noise, but contribute to the density model (Figure 2). We solved the scale selection problem by using a density model trained with empirical data, and templates scaled with tree height (h_{max}). For this experiment, we used 20 Scots pine trees, 24 Norway spruce trees, and 10 deciduous trees. The tree crowns used for training were arbitrarily selected from within the 10 field plots. The extent of the crowns was manually delineated using a DSM derived from the low-altitude laser scanning data and using information about tree classes from the field inventory for tree species annotation. The delineation of tree crowns was used for extraction of laser data from both flight altitudes to produce sensor-specific training data for the templates.

3.2. Tree crown 2D segmentation

The automatic delineation of individual tree crowns to create 2D crown segments requires several steps, which involve using a crown density model for delineation of individual trees: (1) Generate a Canopy Height Model (CHM), (2) create a model fit surface using the best model fit at each raster cell from any of the tested tree crown templates, with height (h_{max}) from the CHM as scaling factor, (3) apply a watershed segmentation to the model fit surface generated in step 2, (4) repeat step 2 including only ALS data from the crown segment resulting from the previous segmentation, and (5) repeat step 3 based on the surface obtained in step 4. In the following five subsections, we describe each of these steps in detail.

3.2.1. Canopy height model

The tree crown 2D segmentation algorithm can use tree heights from any CHM for scaling the templates. However, the CHM should describe the uppermost part of the canopy, excluding low height values or missing data within a tree crown, which otherwise could result in

commission errors. To obtain a suitable CHM with .25 m raster cell size we used morphological filtering to first define crown area and then interpolate crown heights only for raster cells located within areas covered by tree crowns. We describe the process in this subsection. A crown area raster that defined areas covered by the tree crowns was first created using a height threshold (2 m above ground level). The value of a raster cell was set to one if there was at least one laser return above the height threshold within the raster cell, otherwise zero. Morphological closing was then carried out using a 3×3 structuring element. The closing operation involves using dilation followed by erosion. The crown area raster created from the morphological filtering was then used as a mask to construct the canopy height model. A first version of the CHM was created by setting the raster cell values to the maximum height (i.e. distance above the ground) of all laser returns above a height threshold (2 m above ground level) within the raster cell, and to zero if there were no laser returns above the height threshold within the raster cell. The CHM was updated for raster cells with value zero if the crown area raster was equal to one. The new value was calculated by interpolation of values within the smallest window needed to cover at least one raster cell of the first version of the CHM with a value greater than zero.

3.2.2. Model fit surface

We first created a raster that covered the laser-scanned area with a raster cell size of .25 m and set all raster cell values to zero. A model centre was located with its origin at each raster cell centre. The height at the centre of the tree crown model (h_{\max}) was set to the raster cell value of the CHM at the corresponding raster cell. All templates derived in the training phase, one for each tree class, were tested at this location. A measure of model fit, Bhattacharyya coefficient (B), previously also used for segmentation (Ning et al. 2010), was derived for each combination of raster cell location and tree class, using Equation 7, where $p(x_{ij})$ is the relative frequency of laser returns within a raster cell of the crown density raster derived for a tree class in the training phase (Equations 1–6), $q(y_{ij})$ is the relative frequency of laser returns within a raster cell of the local crown density raster derived in the prediction phase (Equations 1–6 applied to data only from the area surrounding the tree centre at the current raster cell location), M is the height (number of rows) and N is the width (number of columns) of the crown density raster. Relative frequency for the models in the training phase and the local model in the prediction phase were derived for each tree class using Equations 8 and 9, respectively, where S_p is the sum of raster cell values in the training phase raster and S_q is the sum of raster cell values in the prediction phase raster. In Equations 8 and 10, x_{ij} is the sum of laser returns in raster cell with index i and j of the crown density raster from the training phase (aggregated from all trees in a specific class used for training) using Equation 6. In Equations 9 and 11, y_{ij} is the number of laser returns in the raster cell with index i and j of the crown density raster from the prediction phase using Equation 6. Thus, B is a measure of model fit with values between zero and one. For the extreme case where the two distributions completely mismatch, B is zero, and for the extreme case where the two distributions completely overlap, B is one.

$$B = \sum_{i=1}^M \sum_{j=1}^N \sqrt{p(x_{ij})q(y_{ij})} \quad (7)$$

$$p(x_{ij}) = x_{ij}/S_p \quad (8)$$

$$q(y_{ij}) = y_{ij}/S_q \quad (9)$$

$$S_p = \sum_{i=1}^M \sum_{j=1}^N x_{ij} \quad (10)$$

$$S_q = \sum_{i=1}^M \sum_{j=1}^N y_{ij} \quad (11)$$

The raster cell value of the MF surface was set to the maximum B value from tests with all models for tree crown classes from the training phase. In this study, three classes were used, namely Scots Pine, Norway spruce, and deciduous trees. The MF surface was smoothed with a 3×3 raster Gaussian filter that was applied recursively three times, in order to avoid local variation caused by noise.

3.2.3. Initial watershed segmentation

A watershed segmentation algorithm was applied to the smoothed MF surface. First, a seed was placed in each raster cell and used as the starting point. Second, a path was derived from each seed to a local maximum. To find this path, the following rule was applied: from one raster cell, move to a neighbouring raster cell in the direction with the steepest slope (eight possible directions), and repeat until a local maximum is reached. All raster cells with seeds that resulted in a path that ended at the same local maximum defined a segment.

3.2.4. Constrained model fit surface

A new MF surface was derived, a Constrained Model Fit (CMF) surface, using the same method as for the first step but with one difference: the local model was derived only from laser returns within the same segment (i.e. from the initial segmentation) as the location of the model tree center (x_c, y_c). The CMF surface was then smoothed with a 3×3 raster Gaussian filter that was applied recursively three times, in order to avoid local variation caused by noise.

3.2.5. Second watershed segmentation

This step involved a second watershed segmentation based on the CMF surface rather than the MF surface. In this step, the algorithm merged segments as not all raster cells were assigned a high B value when only laser data within the segment obtained from the first segmentation were included.

3.3. Tree crown 3D segmentation

The 2D segmentation using 2D model fit surfaces will not detect trees located below other trees. Therefore, we also developed a 3D segmentation algorithm in order to separate the 3D laser returns further into separate tree crowns starting with 3D points in the segment obtained from the 2D surface algorithm. We used the mean shift algorithm for searching 3D cluster centre locations and based our search for cluster centres on the same models of tree crown density as was used

for the 2D segmentation. The generic idea of the mean shift algorithm is as follows, using a simple example with 2D point data. At the location of each 2D point (x, y) , mean values of x and y coordinates are derived using neighbouring 2D points within a specific radius from the current location, giving a new location. For the new location, new mean values of x and y coordinates are derived using 2D points within a radius from this updated location. The procedure is repeated until there is only a small change of locations between subsequent iterations (or until a maximum pre-set number of iterations is reached). In addition, one can use a kernel, for example, a Gaussian function, to calculate weighted mean values, instead of only using mean values within a radius. The mean shift procedure is applied to all the 2D points and the points in the original dataset with updated mean values that arrive to similar locations define a cluster.

3.3.1. Model fit strings

In this work, we used the generic idea of the mean shift algorithm applied to cluster 3D points, and used tree crown density models (i.e. templates) as kernels. These were the same templates as were used for the 2D segmentation. Each crown density raster (i.e. template) was first smoothed with a Gaussian kernel to ensure stable results despite the use of small training datasets. The mean shift algorithm needs a symmetrical kernel in each dimension to avoid centroid locations, updated in each iteration, that depend on the shape of the kernel. However, our templates are symmetrical only in the 2D plane (i.e. radially symmetric). Therefore, in the first step, the centroid location was updated only in the 2D plane, however, still using 3D point data (Equations 12 and 13), where $p(x_{ij})$ was derived using Equation 8, X_t and Y_t are original coordinates, and X_{t+1} and Y_{t+1} are updated coordinates. The location of the center of gravity of the template was used as the kernel center for the mean shift algorithm and the template was scaled with the height. In addition, our crown density model was first smoothed with a Gaussian kernel. In this way, the current mean location was updated in the 2D plane until the change of the mean location (Equation 14) between subsequent iterations was below a threshold of .1 m or until the maximum number of iterations (set to 500) was reached. For each starting point, the mean shift procedure was repeated using each of the templates (i.e. tree class), resulting in one end point for each density model. At the end point, B was calculated (Equation 7) and the end point containing the maximum B , out of all the tested templates, was used together with the maximum B value, for further processing. The mean shift algorithm was applied in the 2D plane using all points in a 2D segment as starting points, each resulting in one end point, with a shift in the 2D plane but not in the vertical direction. Thus, the result of the mean shift in the 2D plane was a set of strings along tree center locations, which consisted of 3D coordinates (i.e. coordinates of end points) and B values, referred to as model fit (MF) strings (Figure 3(a)). We used the name MF strings because these can be sampled and represented as points at any distance from the ground.

$$X_{t+1} = \frac{\sum_{i=1}^M \sum_{j=1}^N p(x_{ij}) X_t}{\sum_{i=1}^M \sum_{j=1}^N p(x_{ij})} \quad (12)$$

$$Y_{t+1} = \frac{\sum_{i=1}^M \sum_{j=1}^N p(x_{ij}) Y_t}{\sum_{i=1}^M \sum_{j=1}^N p(x_{ij})} \quad (13)$$

$$D_{xy} = \sqrt{(X_t - X_{t+1})^2 + (Y_t - Y_{t+1})^2} \quad (14)$$

3.3.2. Clustering of 3D points

Following a MF string from a treetop down toward the ground, the maximum B value is typically found at the centre of a tree crown. Thus, the next step is to follow the MF strings and find one or several local maxima of the B value (i.e. coefficient of model fit). For this final step, the mean shift algorithm was applied in the 3D space using a weighting function that consisted of a product of three terms: (1) Gaussian function of the vertical distance, (2) Gaussian function of the horizontal distance, and (3) the B value (Equation 15). Because of the vertical main direction of the MF strings, we used a high sigma value of the Gaussian function in the vertical direction and a low sigma value of the Gaussian function in the horizontal direction. The sigma values were set as proportions of the z value (i.e. distance to the ground) in order to use higher sigma values at the top of the canopy and lower sigma values close to the ground, using Equations 16 and 17,

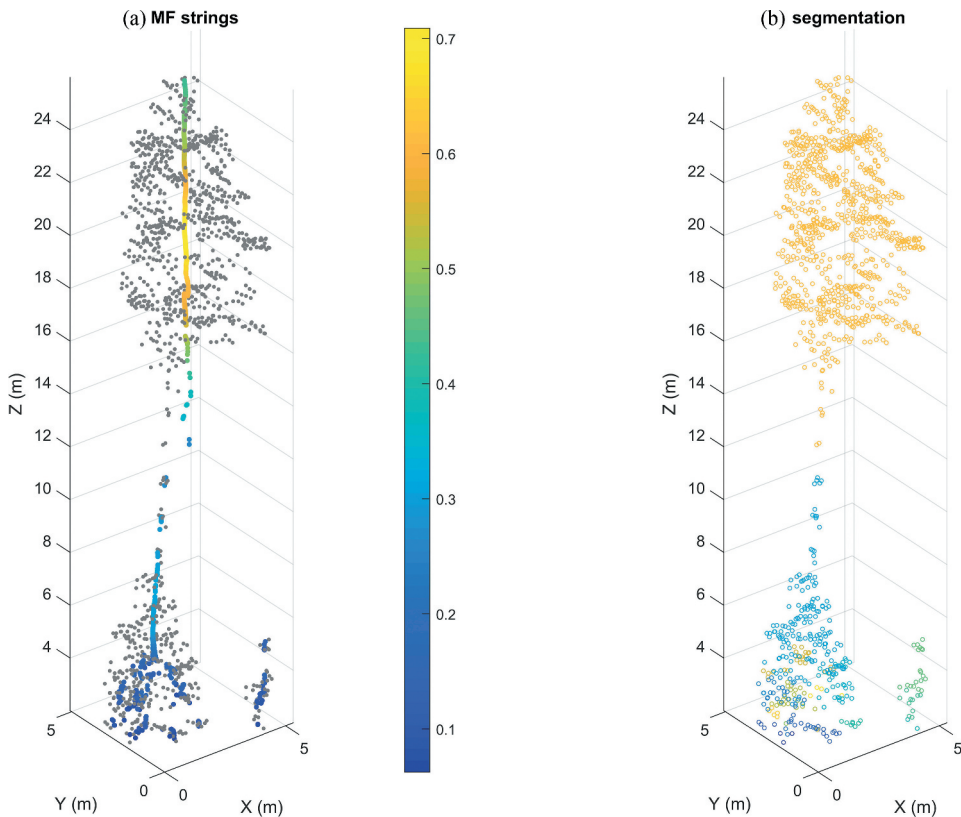


Figure 3. (a) Model fit (MF) strings with colors set by the model fit coefficient (B value) and gray points showing the original point cloud, (b) the original point cloud with colors set by the identification numbers of 3D segments. the original point cloud was selected using a polygon obtained from 2D segmentation using high-altitude ALS data.

where b_r and b_z were set to .05 and .2, respectively. The mean value of the 3D coordinates was updated using the centre locations in the strings (X_c , Y_c , Z_c) inserted into Equations 18–20, where G represents the Gaussian function, and U is the number of 3D points contained in a tree crown polygon according to the 2D segmentation. The mean location was updated in 3D space, following the strings, until the change of the mean location between subsequent iterations (Equation 21) was below a threshold of .1 m, or until a maximum number of iterations (set to 500) was reached. This resulted in a new set of end points along the string cluster centre locations. We clustered the new end points using a threshold for the 3D Euclidian distance (0.3 m). The original 3D coordinates of the laser returns associated with the same cluster using this Euclidian distance clustering were marked with the same cluster identification number (Figure 3(b)).

$$w_i = B_{xyz}G(x, y, \sigma_r)G(z, \sigma_z) \quad (15)$$

$$\sigma_r = b_r Z_t^c \quad (16)$$

$$\sigma_z = b_z Z_t^c \quad (17)$$

$$X_{t+1}^c = \frac{\sum_{i=1}^U w_i X_t^c}{\sum_{i=1}^U w_i} \quad (18)$$

$$Y_{t+1}^c = \frac{\sum_{i=1}^U w_i Y_t^c}{\sum_{i=1}^U w_i} \quad (19)$$

$$Z_{t+1}^c = \frac{\sum_{i=1}^U w_i Z_t^c}{\sum_{i=1}^U w_i} \quad (20)$$

$$D_{xyz} = \sqrt{(X_t^c - X_{t+1}^c)^2 + (Y_t^c - Y_{t+1}^c)^2 + (Z_t^c - Z_{t+1}^c)^2} \quad (21)$$

3.4. Derive attributes for individual trees

The result from the final 2D segmentation was used to estimate tree crown properties. A centre position of a tree crown was estimated using the location of the maximum value of the CMF surface inside the segment. The tree height of a segment was estimated as the maximum laser height within the segment, except in cases where there was tree crown overlap from a neighbouring tree. A segment corresponding to a small tree next to a tall tree could include small areas of the neighbour tree, and therefore have incorrect laser heights near the edge of the tree crown segment. Therefore, the height of the estimated location of the tree crown centre (H_c) was compared with the maximum laser height (H_m) of the segment. If the difference between H_m and H_c was >10% of H_c , we used H_c else H_m was used for the tree height value. The position of a 3D tree crown cluster was

derived using the mean values of x and y coordinates of laser points within the cluster. The height of a 3D tree crown cluster was derived using the 90th percentile of heights (z) for laser points within the cluster.

3.5. Validation

The algorithms (2D segmentation and 3D segmentation) were validated using ALS data from high and low altitudes. In order to increase computation speed, we reduced point density before the 3D clustering step when using the low-altitude ALS data. First, the original point cloud was reduced by using a grid with a voxel size of .1 m and replacing the points within a voxel with new data based on average values. Second, the point cloud used to define start points in the mean shift algorithm and create MF strings was further reduced using the same procedure, but with a voxel size of .2 m. There was a small geometric mismatch between the two sets of ALS data (high and low altitude), which was reduced by matching the DSM from both sensors for each subarea (i.e. field plot) and finding the transformation with the highest correlation between DSM values.

We used automatic linking of field-measured and ALS datasets with an algorithm that minimizes the sum of link distances (Olofsson, Lindberg and Holmgren 2008). The proportion of detected trees was derived as the ratio of linked trees and the total number of manually measured trees in the plot. The proportion of basal area detected was calculated as the sum of basal area (cross-sectional area of the tree stem, 1.3 m above ground level) from linked trees divided by the sum of basal area from all manually measured trees in the plot. The estimated stem volume for each tree was used to derive the sum of stem volume of the detected trees in relation to the sum of stem volume of all the manually measured trees in the field plots.

The commission error was calculated as the proportion of ALS-measured trees that were not linked to a manually measured tree. The stem volumes of trees detected from the ALS data were summed to plot level and compared with the sum of stem volumes of all field measured trees on the plot. For the automatically linked trees detected from the ALS data by the 2D segmentation, the tree heights were compared with the field-measured sample tree heights (i.e. height from ALS minus height from field measurement). Standard deviations of the differences and mean of the differences were calculated. The tree heights derived from ALS data at different flight altitudes were compared using the same procedure.

4. Results

For visualization of the 2D segmentation, tree crown segments were overlaid on a DSM with 5 cm resolution and compared with the manually measured tree positions (Figure 4). The 2D segmentation mostly agreed with both DSM and manually measured trees. For visualization of the 3D clustering, laser returns clustered to tree crowns were represented as 3D points with different colors (Figure 5).

The lowest proportions of detected trees were found for the small trees in field plots with a multi-layered canopy (Figures 6–9, Tables 3–6). When using only 2D segmentation, 87% of the trees were detected from high-altitude ALS data, and 91% of the trees were detected from low-altitude ALS data (Table 7). However, when using 2D segmentation followed by 3D clustering, 92% of the trees were detected using high-altitude ALS data and 99% of the trees were detected using low-altitude ALS data (Table 7). Both flight altitude and choice of algorithm affected the omission error (Table 7). This was especially evident for trees in lower canopy layers (Figures 6–9, Tables 3–6).

The sum of stem volume from the detected trees was compared with the sum of stem volume from all trees within stem diameter intervals. The detected trees represented a high proportion of the stem volume of the field-measured trees (Tables 3–7, undefined Figures 10–13). In order to compare the results of the algorithms developed in this study with a standard tree detection algorithm, we also tested local maximum detection in a DSM with a cell size of .25 m, derived from both high and low altitude ALS data. We used Gaussian smoothing of the DSM and a 2 m search radius to reduce commission errors. The standard algorithm detected 81% of the trees using ALS data from the high altitude, and 82% of the trees using ALS data from the low altitude on average for the plots. The average commission error for the plots was 6% and 5% for high and low altitude ALS data, respectively.

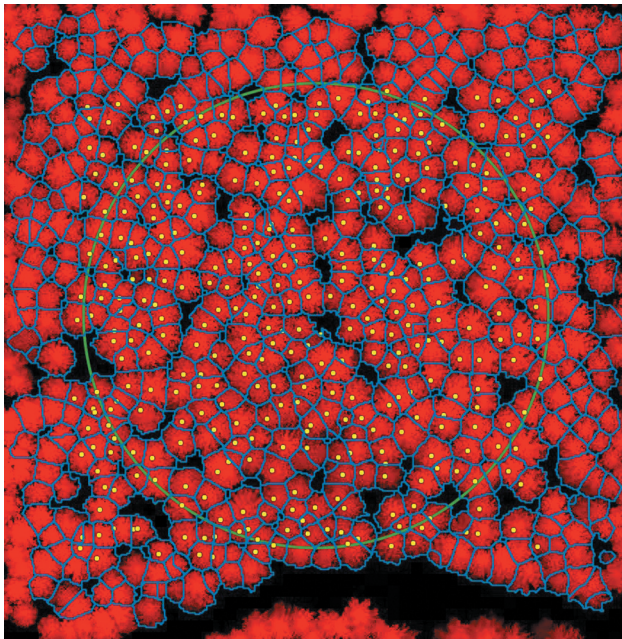


Figure 4. DSM with 0.05 m resolution as the background image, and tree crown segments from the 2D segmentation algorithm using ALS data from low altitude (150 m above ground level) as the input. Field measured tree positions shown as yellow dots. the boundary of the field plot (80 m diameter) is shown with a green circle.

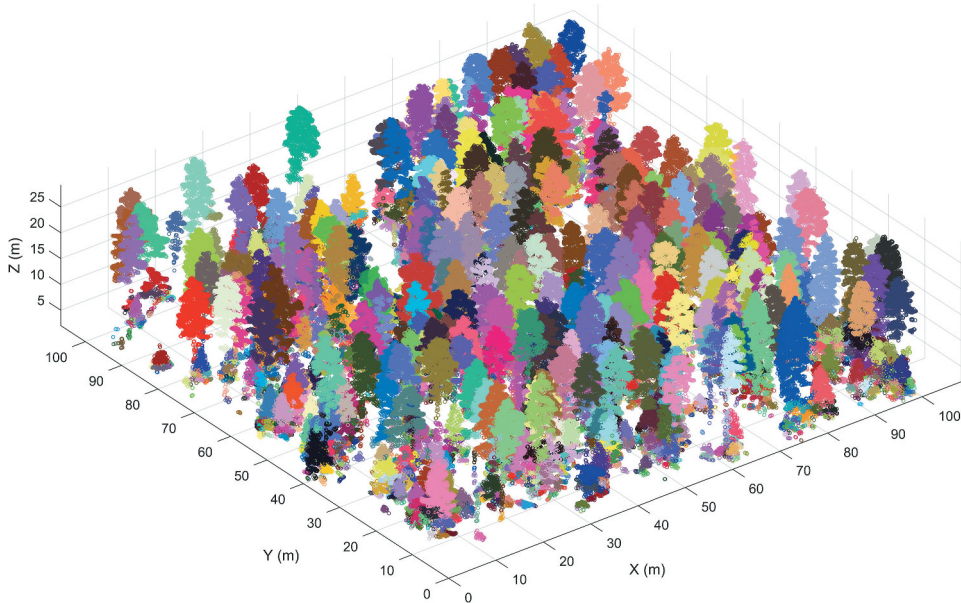


Figure 5. Clustering of 3D point cloud produced from high-altitude ALS data (1450 m above ground level).

When comparing DSM from the first (low altitude) and second scanning (high altitude) missions, we observed that several trees had been removed between the scanning events, especially in plot 2. This could be one reason for the lower detection rate in the high-altitude scanning, when compared with earlier field data. There were many commission errors in a few plots, especially plot number 9. After comparing field data, DSM and segmentation, it was clear that many small trees were detected from the ALS data that were not measured during the field inventory. This was probably due to the limit of 4 cm DBH for manual field measurements of a tree while the lower threshold used by the algorithms was 2 m height in the ALS data. The reported commission errors were reduced when we only included tall trees (>10 m ALS height) for the validation. Thresholds using different variables (stem diameter from field inventory and height from ALS) will increase the magnitude of reported commission errors compared to true commission errors. For tall trees (>10 m ALS height) and for the 2D segmentation, the commission error was between 5% and 17% using high-altitude ALS data (Table 3), and between 3% and 10% using low-altitude ALS data (Table 4). After comparing field data and DSM, it was clear that a few trees in each plot were missed during the manual field inventory. Trees excluded during the field inventory contribute to the total commission errors.

Tree height estimates from the two different ALS acquisitions were compared (Figure 14). In addition, tree height estimates from high-altitude ALS and low-altitude ALS data were compared with manual measurements (Figures 15 and 16). The standard deviation of differences between trees heights from ALS from two different altitudes was .73 m. The bias was .24 m, thus tree heights were, on average, estimated to be lower from the higher altitude data (Figure 14). The standard deviation of differences between ALS-

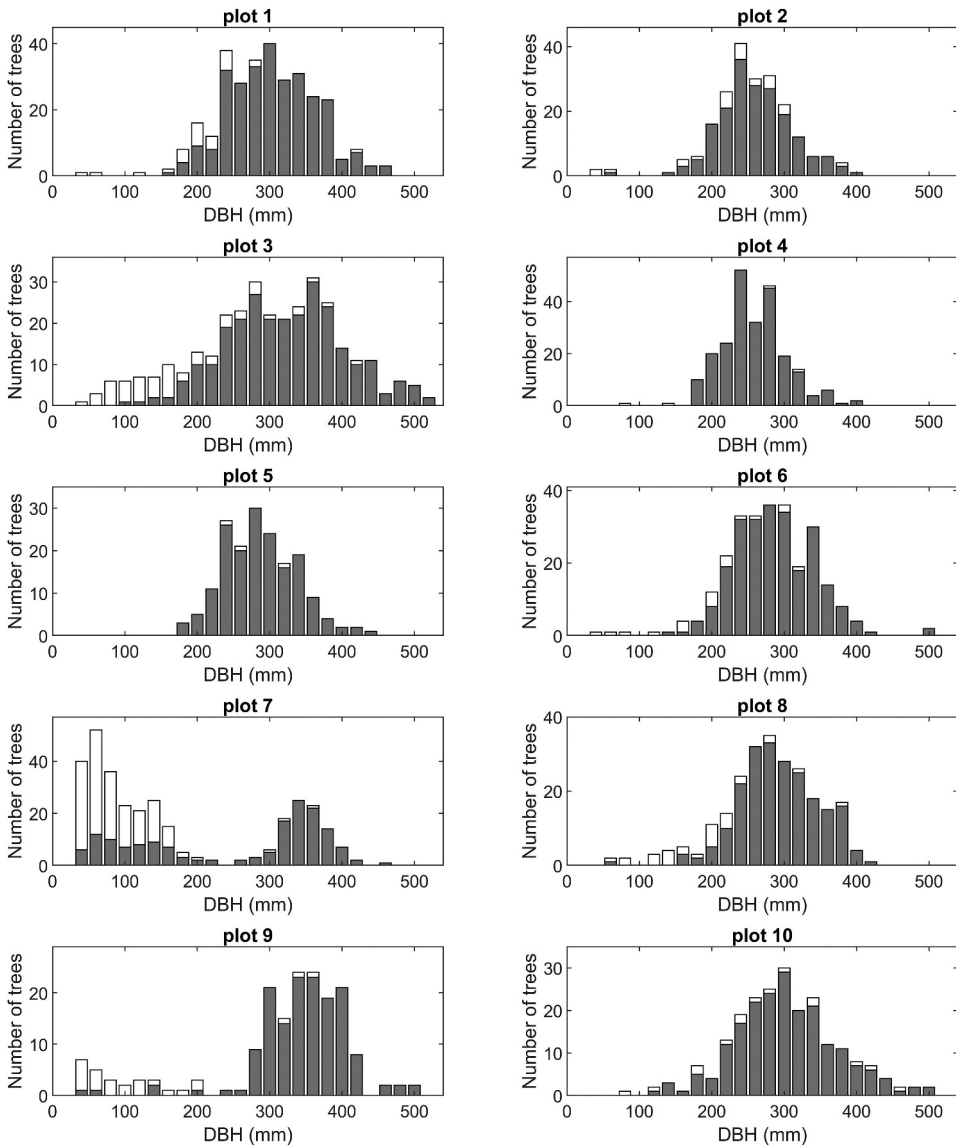


Figure 6. Histograms showing tree detection results from 2D segmentation using high-altitude ALS data (white bars for all field trees and gray bars for field trees that were linked to trees detected in the ALS data).

measured heights from the higher altitude and field-measured tree heights was .86 m. The bias was $-.07$ m, thus tree heights were, on average, estimated to be lower from ALS data than from manual measurements (Figure 15). The standard deviation of differences between ALS-measured heights from the lower altitude and field-measured tree heights was .74 m. The bias was .13 m, thus tree heights were, on average, estimated to be higher from ALS data than from manual measurements (Figure 16).

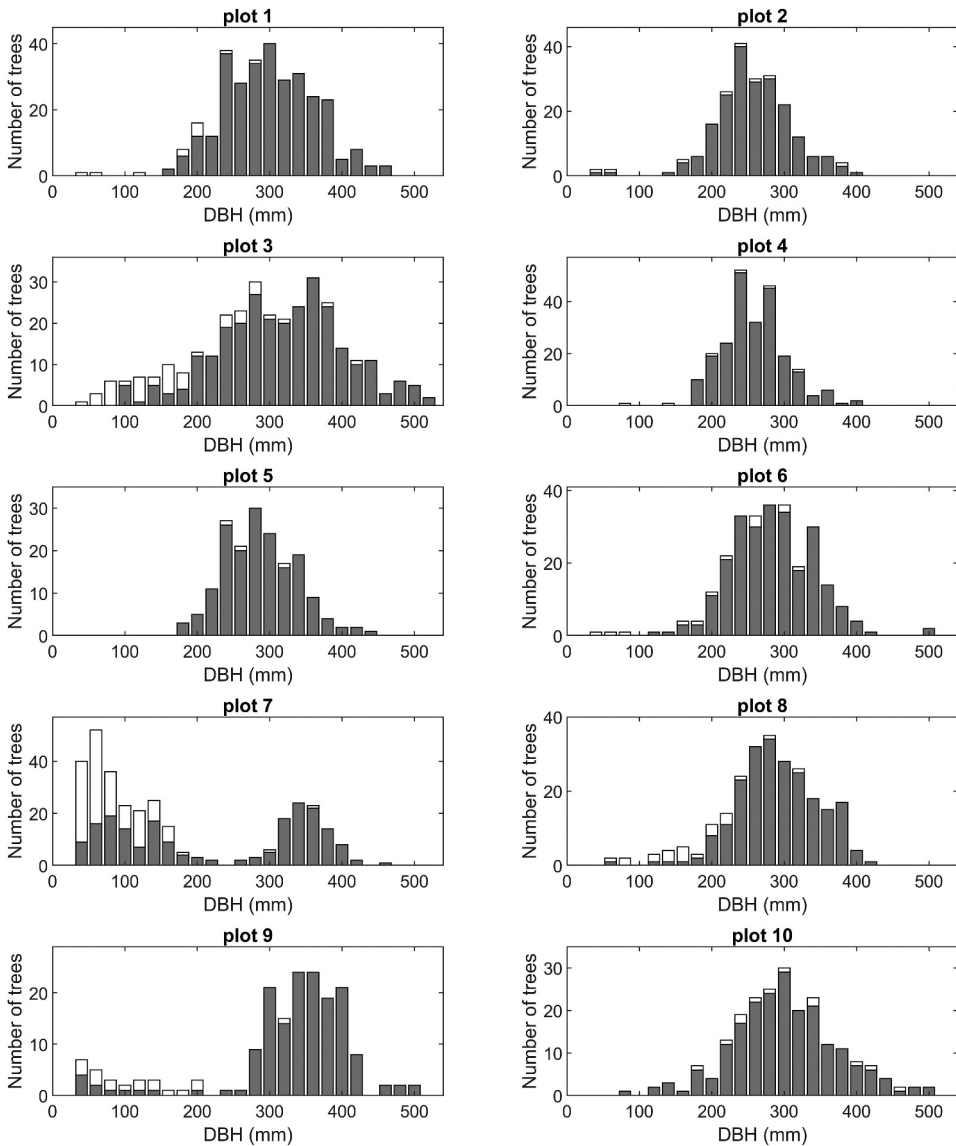


Figure 7. Histograms showing tree detection results from 2D segmentation using low-altitude ALS data (white bars for all field trees and gray bars for field trees that were linked to tree detected in the ALS data).

5. Discussion

We have developed new segmentation algorithms, which uses density models of tree crowns with empirical data as a reference. Axelsson (1999) highlighted the advantage of using original laser data in the filtering and modelling process. For the algorithms, we model tree crowns using original laser data. We search for tree locations and carry out delineation of trees with a watershed algorithm, where the input is a model fit surface instead of a canopy height surface model. We solve the

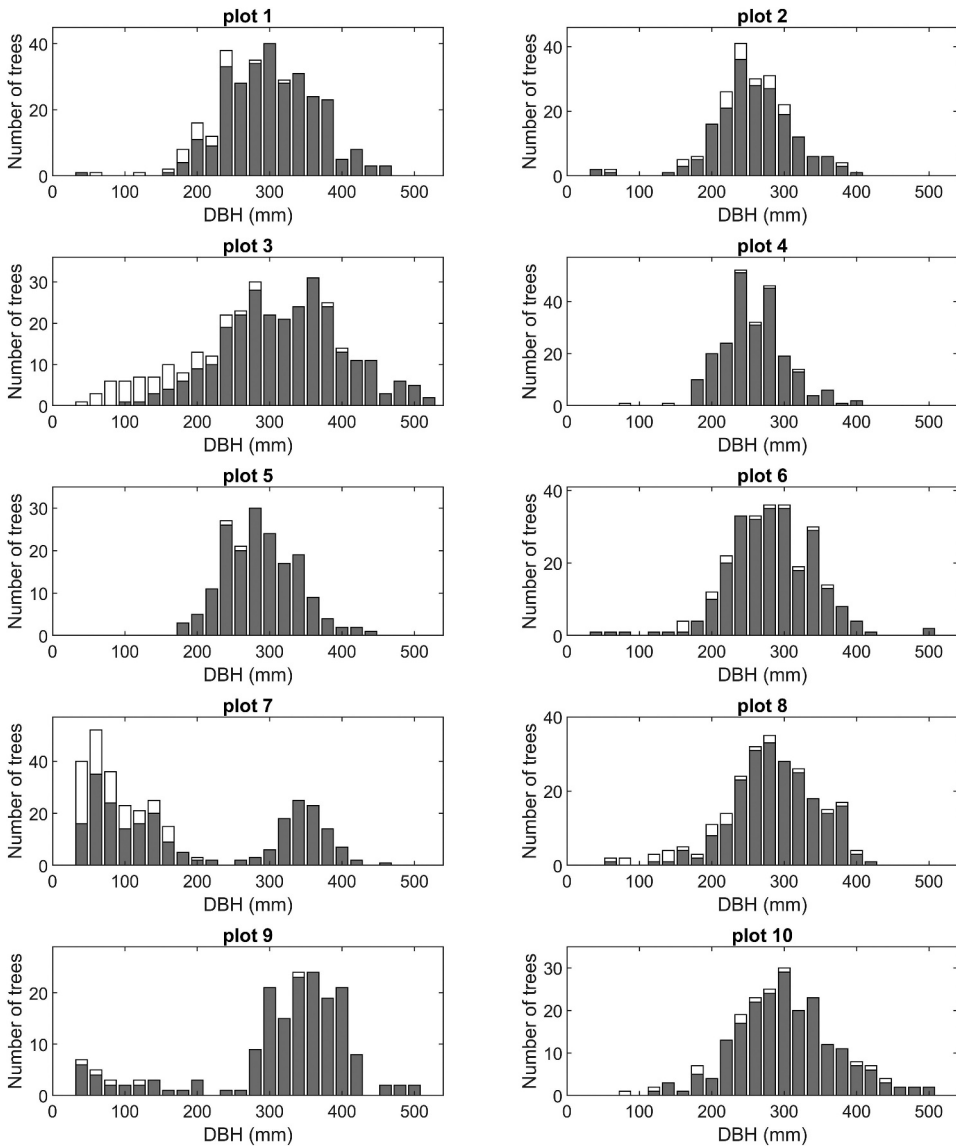


Figure 8. Histograms showing 3D segmentation tree detection results using high-altitude ALS data (white bars for all field trees and gray bars for field trees that were linked to tree detected in the ALS data).

scale selection problem using a training phase, where we create crown density models for a set of tree classes. The simple models, with scaling using tree heights and an assumption of radial symmetry, reduce the amount of data needed for training and make the algorithm computationally efficient. The algorithm does not require site-specific parameter settings. Instead, the algorithm learns from laser data using manually delineated tree crown polygons (empirical data). These polygons should be defined for tree crown classes, where trees of the same class have similar crown shape and structure. In this study, we only used three classes and

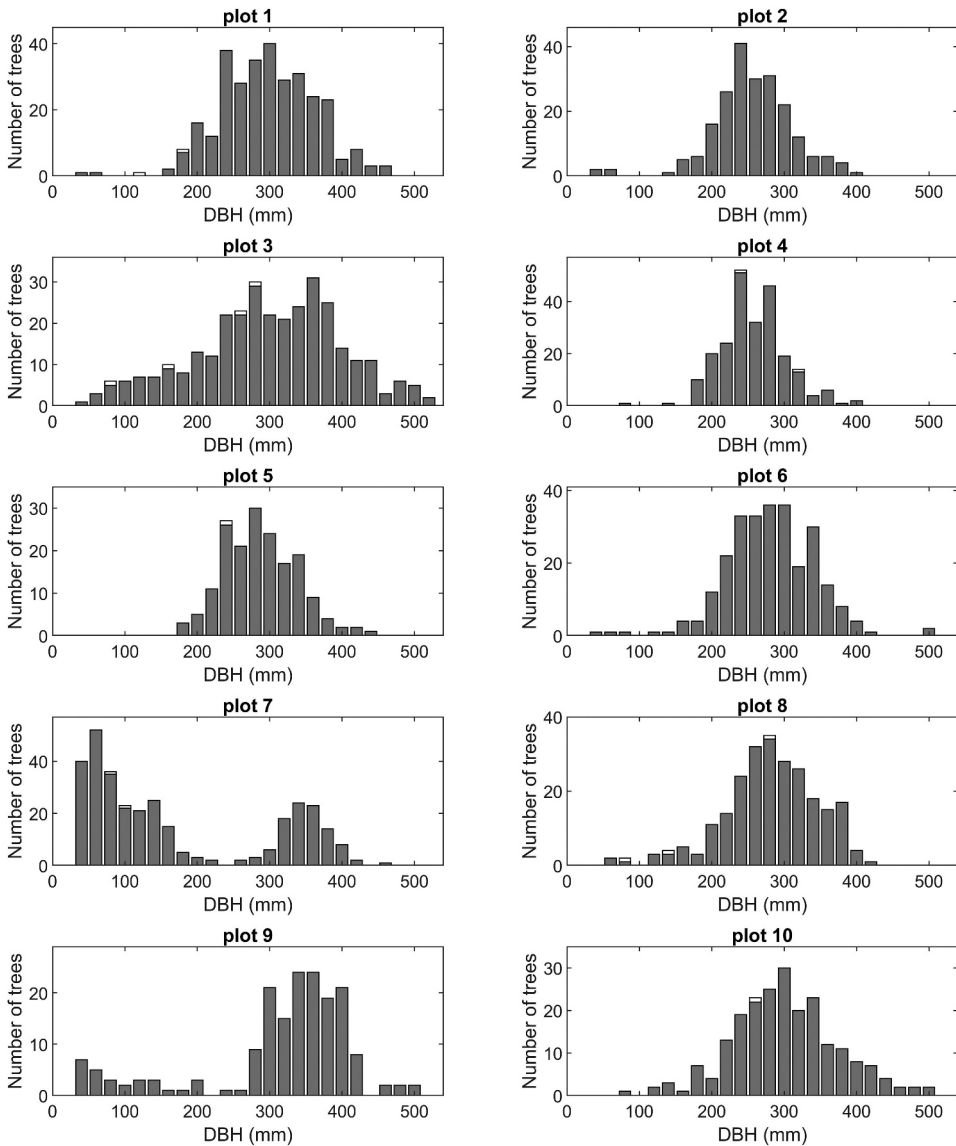


Figure 9. Histograms showing 3D segmentation tree detection results using low-altitude ALS data (white bars for all field trees and gray bars for field trees that were linked to tree detected in the ALS data).

a few trees within each tree class. Future work should find out how segmentation results depend on training data size and number of tree species.. More efficient procedures should be developed for selection of empirical data. In addition, future work should find out potential errors due to inclusion of data from low vegetation in the models.

The use of a model fit surface makes it difficult to detect trees located below other trees. Therefore, we used 3D clustering as an optional second step, which requires more computations. For the 3D clustering, we first use the mean shift

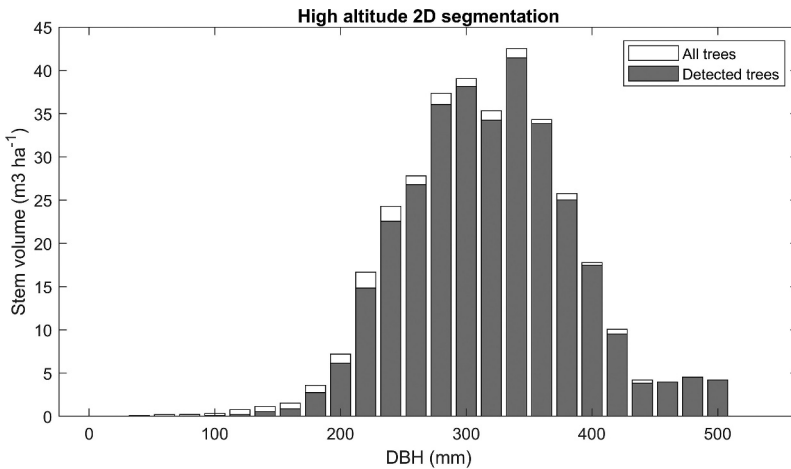


Figure 10. Stem volume for all trees and for detected trees using high-altitude 2D segmentation in stem diameter intervals on all field plots.

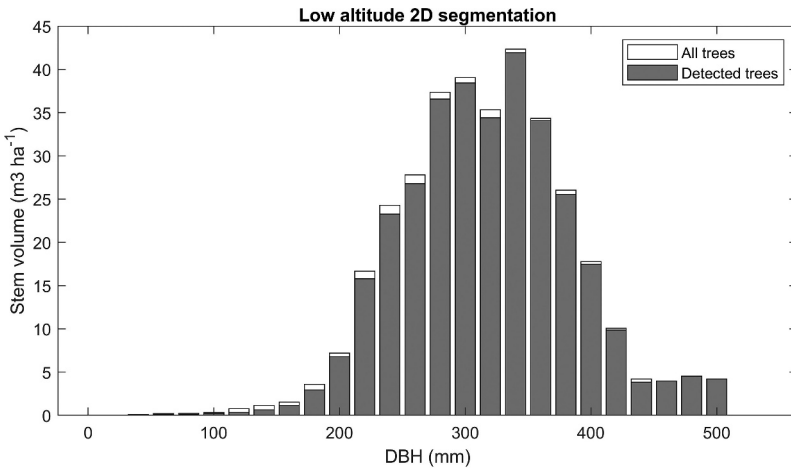


Figure 11. Stem volume for all trees and for detected trees using low-altitude 2D segmentation in stem diameter intervals on all field plots.

algorithm in two dimensions, with density models of tree crowns as kernels, to find strings that define the centre locations of tree crowns, and derive model fit coefficients for each part of these strings. We then apply the mean shift algorithm in three dimensions to find local maxima of coefficients along the strings to define cluster centres. Although the sequential approach with 2D segmentation followed by 3D clustering was successful in earlier studies it will introduce problems. For example, the restriction of the 3D clustering to use only data from a 2D segment will yield incorrect clusters if the 2D segmentation has errors. In this study, the 3D clustering was strictly limited to a 2D segment, i.e. the 3D clustering was first performed with data from one 2D segment, and then using data from another 2D segment. Although the 3D clustering is able to detect several small trees located

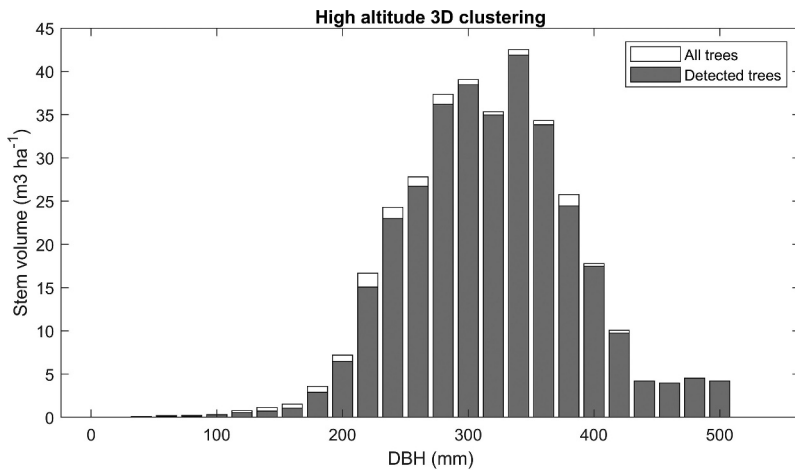


Figure 12. Stem volume for all trees and for detected trees using high-altitude 3D segmentation in stem diameter intervals on all field plots.

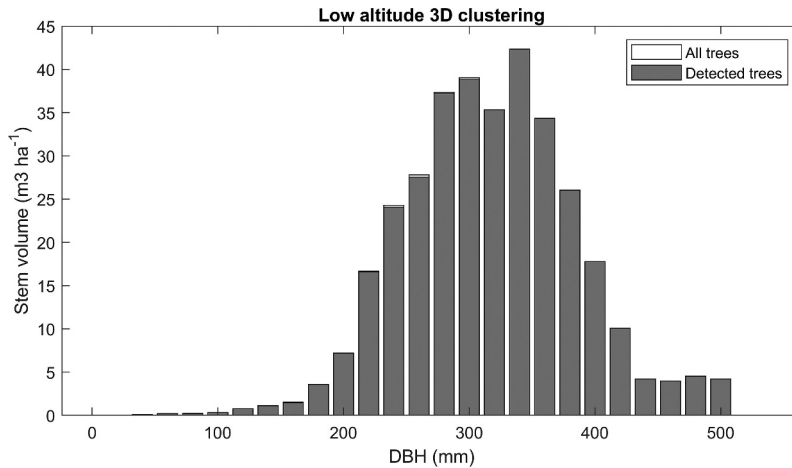


Figure 13. Stem volume for all trees and for detected trees using low-altitude 3D segmentation in stem diameter intervals on all field plots.

Table 3. Results from tree detection using 2D segmentation and high-altitude ALS data: omission errors affect (in percentage) on the number of trees (Number), on the basal area (Basal area), and on the stem volume (Volume); commission error (in percentage) of all trees and of only tall trees (ALS tree height >10 m).

Plot	Omission error (%)			Commission error (%)	
	Number	Basal area	Volume	All trees	Tall trees
1	9	5	4	9	8
2	12	10	9	7	7
3	17	7	6	10	10
4	2	1	1	6	5
5	2	2	1	13	8
6	7	4	3	11	9
7	49	11	8	17	12
8	12	6	5	12	11
9	15	3	3	34	17
10	7	6	6	13	13

Table 4. Results from tree detection using 2D segmentation and low-altitude ALS data: omission errors affect (in percentage) on the number of trees (Number), on the basal area (Basal area), and on the stem volume (Volume); commission error (in percentage) of all trees and of only tall trees (ALS tree height >10 m).

Plot	Omission error (%)			Commission error (%)	
	Number	Basal area	Volume	All trees	Tall trees
1	4	1	1	5	4
2	4	3	3	4	3
3	14	5	4	6	6
4	3	2	2	7	4
5	2	2	2	11	3
6	5	3	3	7	5
7	38	8	5	15	3
8	9	4	3	5	4
9	10	2	1	46	7
10	5	6	5	10	10

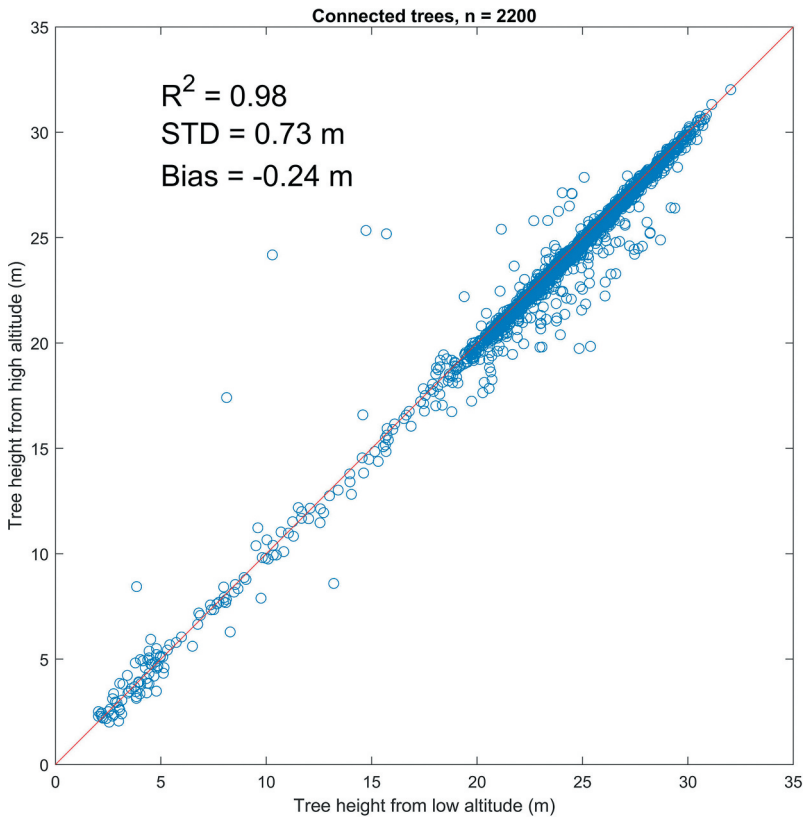


Figure 14. Tree heights from high-altitude ALS data (1450 m above ground level) and tree heights from low-altitude ALS data (150 m above ground level) for automatically connected trees on 10 sample plots (2200 linked trees), coefficient of determination (R^2), standard deviation of differences (STD) and mean value of differences (Bias).

Table 5. Results from tree detection using 3D segmentation and high-altitude ALS data: omission errors affect (in percentage) on the number of trees (Number), on the basal area (Basal area), and on the stem volume (Volume); commission error (in percentage) of all trees and of only tall trees (ALS tree height >10 m).

Plot	Omission error (%)			Commission error (%)	
	Number	Basal area	Volume	All trees	Tall trees
1	7	3	3	17	7
2	11	10	9	21	8
3	15	5	4	23	10
4	3	2	2	15	6
5	1	1	1	35	8
6	5	4	4	26	10
7	24	4	3	41	17
8	10	6	6	28	11
9	3	1	1	69	23
10	5	5	4	31	14

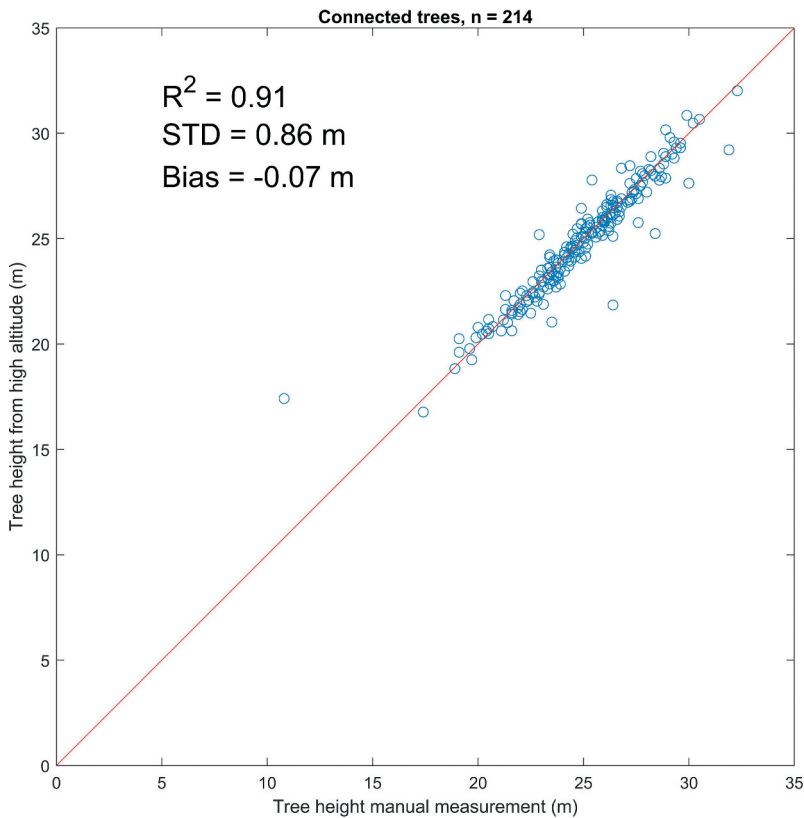


Figure 15. Tree heights from individual trees obtained from high-altitude ALS data (1450 m above ground level) and field-measured trees (214 linked trees), coefficient of determination (R^2), standard deviation of differences (STD) and mean value of differences (Bias).

Table 6. Results from tree detection using 3D segmentation and low-altitude ALS data: omission errors affect (in percentage) on the number of trees (Number), on the basal area (Basal area), and on the stem volume (Volume); commission error (in percentage) of all trees and of only tall trees (ALS tree height >10 m).

Plot	Omission error (%)			Commission error (%)	
	Number	Basal area	Volume	All trees	Tall trees
1	1	0	0	61	5
2	0	0	0	67	3
3	1	1	0	66	7
4	1	1	1	62	4
5	1	0	0	67	3
6	0	0	0	73	6
7	1	0	0	81	25
8	1	1	0	72	6
9	0	0	0	92	45
10	0	0	0	77	14

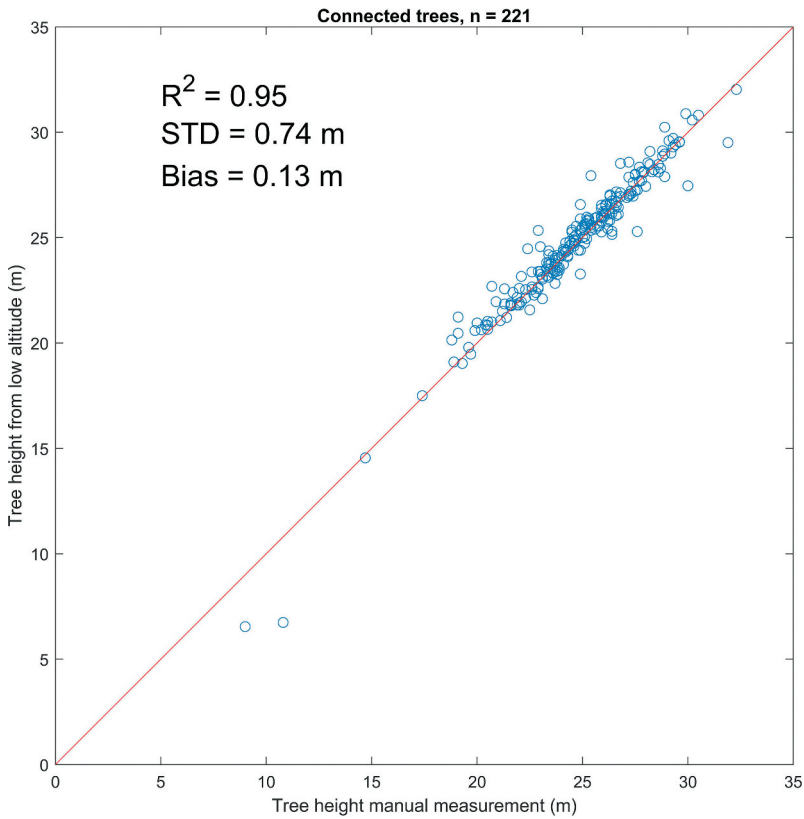


Figure 16. Tree heights for individual trees obtained from a helicopter at low altitude (150 m above ground level) and field-measured trees (221 linked trees), coefficient of determination (R^2), standard deviation of differences (STD) and mean value of differences (Bias).

Table 7. Mean values of plot results from tree detection using 2D segmentation and low-altitude ALS data: omission errors affect (in percentage) on the number of trees (number), on the basal area (basal area), and on the stem volume (volume); commission error (in percentage) of all trees and of only tall trees (ALS tree height >10 m).

Dataset	Algorithm	Omission error (%)			Commission error (%)	
		Number	Basal area	Volume	All trees	Tall trees
High altitude	2D segmentation	13	6	5	13	10
Low altitude	2D segmentation	9	4	3	12	5
High altitude	3D segmentation	8	4	4	31	11
Low altitude	3D segmentation	1	0	0	72	12

below a tall tree, problems will occur if several tall trees (i.e. several 2D segments) cover one small tree. It is possible to solve this problem using buffer zones of ALS data outside the currently processed 2D segment and only save 3D clusters with their centres located within the currently processed 2D segment. The results of the 3D clustering was limited to modelling of tree crowns. One effect of this can be observed in [Figure 3\(b\)](#), where data from a tree stem belonging to a tall tree was included in the 3D cluster of a shorter tree below. This will result in an over-estimated tree height for the shorter tree, which might be one reason for relatively high commission errors observed on two plots with a mixture of tall pine trees and short trees ([Tables 5-6](#)). It is possible to solve this problem by also detecting tree stems, and not only tree crowns.

Some trees were removed between the two ALS data acquisition missions, probably due to bark beetle infestation. The removals were clear when comparing the DSM from the two different ALS datasets. Thus, the true proportions of detected trees, using high-altitude ALS data, are higher than given by the comparison with field data. The field measurements used for validation were not completely correct. This was due to field crews sometimes making mistakes. For example, one field crew omitted some trees from the inventory. They painted the trees that had been measured in order to avoid this mistake. Despite painting the trees, some errors in the field measurements are visible when comparing field measurements to a DSM with 5 cm resolution, and therefore contribute to the commission error. Thus, true commission errors are lower compared to the values from the validation based on the field inventory.

We also experienced problems using different thresholds for the different data sources, that is, stem diameter (DBH) for the field inventory and height for the ALS data. One solution to the threshold problem was to use only tall trees for validation of commission errors. For tall trees, commission errors were smaller, and trees missed during the field inventory can explain some of the errors. However, the commission errors were larger for the high-altitude ALS data. One reason for larger commission errors using lower resolution ALS data could be lower quality of the canopy height model used to set the height of tree crown models. We used morphological filters to derive a canopy area raster, which we used to decide whether we should interpolate height values for data raster cells with no data values in the canopy height model (CHM). Problems with raster cell values in the

CHM deviating from the true canopy height could be one reason for larger commission errors when using ALS data with lower density, and it could therefore be possible to improve the results using enhanced interpolation.

We observed similar proportions of detected volume for the two ALS data resolutions. The detection rates in lower canopy layers were higher using high-resolution ALS data. In earlier studies, tree detection results have been similar, compared to results obtained in this study, for densities above 10 laser returns per square meter (Reitberger et al. 2009; Kaartinen et al. 2012; Yao et al. 2014; Kandare et al. 2016). We observed a high proportion of detected trees in this study, using low-altitude ALS data and 3D segmentation, compared to several earlier studies. However, the results are difficult to compare because of the use of different data for validation.

In this study, we compared tree height estimates from two altitudes. The standard deviation of the differences was .73 m. Morsdorf et al. (2008) observed a small difference in tree height estimates using ALS from flight altitudes of 500 m and 900 m above ground level. For comparison with manual measurements, the standard deviation was only slightly higher using ALS data from 900 m altitude, 1.49 m, compared with 1.39 m for the 500 m altitude. In comparisons of several algorithms in Finland using ALS data from 600 m flight altitude and ALS data densities of 2, 4, and 8 points per m², the root-mean-square errors of tree height estimations were usually between .5 m and 1.0 m (Kaartinen et al. 2012) which are similar to the results obtained in our study.

Very high-resolution ALS makes it possible to obtain laser returns from all treetops not obscured by other trees. There are errors caused by manual measurements using a hypsometer for angle measurement and from problems in observing treetops from a location on the ground. Therefore, the reported errors from ALS-based estimates of tree height could depend much on the errors caused by the manual method used for validation. For example, tree heights from ALS from a low altitude were on average higher than from manual measurements, which could be a result of problems to observe all parts of the treetop from a viewpoint on the ground.

6. Conclusions

We observed higher tree detection rates using ALS data collected from low altitude (150 m above ground level) compared to high altitude (1450 m above ground level). The algorithm produced similar results using high-altitude ALS data compared to low-altitude ALS data for detection of trees that made up the majority of the total stem volume. Thus, the high-resolution ALS data from a low altitude was mostly useful for detection of small trees in lower vegetation layers. The second part of the algorithm included clustering of 3D point data, making it possible to detect trees located below other trees. However, this second part is more computationally expensive. High proportions of the stem volume were detected with only the first part of the algorithm, using watershed segmentation of a model fit surface. This is important information for large-area mapping of forest resources in terms of wood supply to forest industries. However, low-altitude ALS data can be used to produce high-resolution point clouds for detailed

mapping of specific areas and provide additional information about low vegetation; this information is useful for environmental monitoring of hot-spot areas or for planning forest operations. The use of 3D tree crown segmentation based on crown density models made it possible to detect a large percentage of trees in multi-layered forests.

Acknowledgements

COWI Mapping (now Hexagon Geosystems) performed the high-altitude laser scanning and Visimind AB performed the low-altitude laser scanning. The authors would like to thank the field crew who collected the data used for validation.

Disclosure statement

No potential conflict of interest was reported by the author(s).

Funding

The work was supported by the Bo Rydins Foundation for Science Research [F19/17]; Brattås Foundation for Forest Science Research [F18:03]; Carl Tryggers Foundation for Science Research [CTS 18: 151]; The Royal Swedish Academy of Agriculture and Forestry (KSLA) [TF 2019-0064]; Hildur and Sven Wingquist Foundation for Forest Science Research [17/18-2 / 107-5 SOJOH,18/19-4 / 110-5 SOJOH]; Skogssällskapet [2019-649-S2 2018 LIABE]; FORMAS [2018-01161].

ORCID

Johan Holmgren  <http://orcid.org/0000-0002-7112-8015>

Eva Lindberg  <http://orcid.org/0000-0002-1792-0773>

Kenneth Olofsson  <http://orcid.org/0000-0002-2836-2316>

Henrik J. Persson  <http://orcid.org/0000-0002-3403-057X>

References

- Axelsson, P. E. 1999. "Processing of Laser Scanner Data—algorithms and Applications." *ISPRS Journal of Photogrammetry and Remote Sensing* 54 (2–3): 138–147. doi:10.1016/S0924-2716(99)00008-8.
- Baltsavias, E. P. 1999. "Airborne Laser Scanning: Basic Relations and Formulas." *ISPRS Journal of Photogrammetry and Remote Sensing* 54 (2–3): 199–214. doi:10.1016/S0924-2716(99)00015-5.
- Bian, Y., P. Zou, Y. Shu, and Y. Ronghuan. 2014. "Individual Tree Delineation in Deciduous Forest Areas with LiDAR Point Clouds." *Canadian Journal of Remote Sensing* 40 (2): 152–163.
- Brandel, G. 1990. *Volume Functions for Individual Trees : Scots Pine (Pinus Sylvestris), Norway Spruce (Picea Abies) and Birch (Betula Pendula & Betula Pubescens)*. Garpenberg, Sweden: Swedish University of Agricultural Sciences.
- Bucksch, A., R. Lindenbergh, M. Zulkarnain Abd Rahman, and M. Menenti. 2013. "Breast Height Diameter Estimation from High-Density Airborne LiDAR Data." *IEEE Geoscience and Remote Sensing Letters* 11 (6): 1056–1060. doi:10.1109/LGRS.2013.2285471.

- Falkowski, M. J., A. M. S. Smith, A. T. Hudak, P. E. Gessler, L. A. Vierling, and N. L. Crookston. 2006. "Automated Estimation of Individual Conifer Tree Height and Crown Diameter via Two-Dimensional Spatial Wavelet Analysis of Lidar Data." *Canadian Journal of Remote Sensing* 32 (2): 153–161. doi:10.5589/m06-005.
- Gupta, S., H. Weinacker, and B. Koch. 2010. "Comparative Analysis of Clustering-Based Approaches for 3-D Single Tree Detection Using Airborne Fullwave Lidar Data." *Remote Sensing* 2 (4): 968–989. doi:10.3390/rs2040968.
- Holmgren, J. and E. Lindberg. 2013. "Tree Crown Segmentation Based on a Geometric Tree Crown Model for Prediction of Forest Variables." *Canadian Journal of Remote Sensing* 39 (sup1): S86–S98. doi:10.5589/m13-025.
- Holmgren, J. and E. Lindberg. 2019. "Tree Crown Segmentation Based on a Tree Crown Density Model Derived from Airborne Laser Scanning." *Remote Sensing Letters* 10 (12): 1143–1152. doi:10.1080/2150704X.2019.1658237.
- Holopainen, M., M. Vastaranta, and J. Hyypä. 2014. "Outlook for the Next Generation's Precision Forestry in Finland." *Forests* 5 (7): 1682–1694. doi:10.3390/f5071682.
- Hyypä, J., H. Hyypä, D. Leckie, F. Gougeon, X. Yu, and M. Maltamo. 2008. "Review of Methods of Small-Footprint Airborne Laser Scanning for Extracting Forest Inventory Data in Boreal Forests." *International Journal of Remote Sensing* 29 (5): 1339–1366. doi:http://dx.doi.org/10.1080/01431160701736489.
- Kaartinen, H., J. Hyypä, X. Yu, M. Vastaranta, H. Hyypä, A. Kukko, and M. Holopainen, Heipke, C., Hirschmugl, M., Morsdorf, F., Næsset, E., Pitkänen, J., Popescu, S., Solberg, S., Wolf, B.M., Wu, J. et al.2012. "An International Comparison of Individual Tree Detection and Extraction Using Airborne Laser Scanning." *Remote Sensing* 4 (4): 950–974. doi:http://dx.doi.org/10.3390/rs4040950.
- Kandare, K., H. Ole Ørka, J.-C.-W. Chan, and M. Dalponte. 2016. "Effects of Forest Structure and Airborne Laser Scanning Point Cloud Density on 3D Delineation of Individual Tree Crowns." *European Journal of Remote Sensing* 49 (1): 337–359. doi:10.5721/EuJRS20164919.
- Kellner, J. R., J. Armston, K. C. Markus Birrer, L. Duncanson, C. Eck, C. Fallegger, B. Imbach, K. Král, and M. Krůček. 2019. "New Opportunities for Forest Remote Sensing Through Ultra-High-Density Drone Lidar." *Surveys in Geophysics* 40 (4): 959–977. doi:10.1007/s10712-019-09529-9.
- Lee, H., K. Clint Slatton, B. Edward Roth, and W.P. Cropper Jr.2010. "Adaptive Clustering of Airborne LiDar Data to Segment Individual Tree Crowns in Managed Pine Forests." *International Journal of Remote Sensing* 31 (1): 117–139. doi:10.1080/01431160902882561.
- Lindberg, E. and J. Holmgren. 2017. "Individual Tree Crown Methods for 3D Data from Remote Sensing." *Current Forestry Reports* 3 (1): 19–31. doi:10.1007/s40725-017-0051-6.
- Lindberg, E., L. Eysn, M. Hollaus, J. Holmgren, and N. Pfeifer. 2014. "Delineation of Tree Crowns and Tree Species Classification from Full-Waveform Airborne Laser Scanning Data Using 3-D Ellipsoidal Clustering." *Ieee Journal of Selected Topics in Applied Earth Observations and Remote Sensing* 7 (7): 3174–3181. doi:10.1109/jstars.2014.2331276.
- Lu, X., Q. Guo, W. Li, and J. Flanagan. 2014. "A Bottom-Up Approach to Segment Individual Deciduous Trees Using Leaf-off Lidar Point Cloud Data." *ISPRS Journal of Photogrammetry and Remote Sensing* 94: 1–12. doi:10.1016/j.isprsjprs.2014.03.014.
- Mongus, D. and B. Žalik. 2015. "An Efficient Approach to 3D Single Tree-Crown Delineation in LiDar Data." *ISPRS Journal of Photogrammetry and Remote Sensing* 108: 219–233. doi:10.1016/j.isprsjprs.2015.08.004.
- Morsdorf, F., E. Meier, B. Allgöwer, and D. Nüesch. 2003. "Clustering in Airborne Laser Scanning Raw Data for Segmentation of Single Trees." *International Archives of the Photogrammetry, Remote Sensing and Spatial Information Sciences* 34 (part 3): W13.
- Morsdorf, F., O. Frey, E. Meier, K. I. Itten, and B. Allgower. 2008. "Assessment of the Influence of Flying Altitude and Scan Angle on Biophysical Vegetation Products Derived from Airborne Laser Scanning." *International Journal of Remote Sensing* 29 (5): 1387–1406. doi:10.1080/01431160701736349.

- Nilsson, M., K. Nordkvist, J. Jonzen, N. Lindgren, P. Axensten, J. Wallerman, and M. Egberth, Larsson, S., Nilsson, L., Eriksson, J., Olsson, H. 2017. "A Nationwide Forest Attribute Map of Sweden Predicted Using Airborne Laser Scanning Data and Field Data from the National Forest Inventory." *Remote Sensing of Environment* 194: 447–454. doi:[10.1016/j.rse.2016.10.022](https://doi.org/10.1016/j.rse.2016.10.022).
- Ning, J., L. Zhang, D. Zhang, and C. Wu. 2010. "Interactive Image Segmentation by Maximal Similarity Based Region Merging." *Pattern Recognition* 43 (2): 445–456. doi:[10.1016/j.patcog.2009.03.004](https://doi.org/10.1016/j.patcog.2009.03.004).
- Olofsson, K., E. Lindberg, and J. Holmgren. 2008. A Method for Linking Field-Surveyed and Aerial-Detected Single Trees Using Cross Correlation of Position Images and the Optimization of Weighted Tree List Graphs. Paper presented at the Proceedings of SilviLaser 2008, 8th international conference on LiDAR applications in forest assessment and inventory, Heriot-Watt University, Edinburgh, UK, September 17–19.
- Persson, Å., J. Holmgren, and U. Söderman. 2002. "Detecting and Measuring Individual Trees Using an Airborne Laser Scanner." *Photogrammetric Engineering and Remote Sensing* 68: 925–932.
- Persson, H. J. and J. E. Fransson. 2017. "Comparison Between TanDem-X-and ALS-Based Estimation of Aboveground Biomass and Tree Height in Boreal Forests." *Scandinavian Journal of Forest Research* 32 (4): 306–319. doi:[10.1080/02827581.2016.1220618](https://doi.org/10.1080/02827581.2016.1220618).
- Popescu, S. C., R. H. Wynne, and R. F. Nelson. 2002. "Estimating Plot-Level Tree Heights with Lidar: Local Filtering with a Canopy-Height Based Variable Window Size." *Computers and Electronics in Agriculture* 37 (1–3): 71–95. doi:[10.1016/S0168-1699\(02\)00121-7](https://doi.org/10.1016/S0168-1699(02)00121-7).
- Reitberger, J., C. Schnorr, P. Krzystek, and U. Stilla. 2009. "3D Segmentation of Single Trees Exploiting Full Waveform LIDAR Data." *ISPRS Journal of Photogrammetry and Remote Sensing* 64 (6): 561–574. doi:[10.1016/j.isprsjprs.2009.04.002](https://doi.org/10.1016/j.isprsjprs.2009.04.002).
- Swatantran, A., H. Tang, T. Barrett, P. DeCola, and R. Dubayah. 2016. "Rapid, High-Resolution Forest Structure and Terrain Mapping Over Large Areas Using Single Photon Lidar." *Scientific Reports* 6.
- Vaughn, N. R., L. M. Moskal, and E. C. Turnblom. 2012. "Tree Species Detection Accuracies Using Discrete Point Lidar and Airborne Waveform Lidar." *Remote Sensing* 4 (2): 377–403. doi:[10.3390/rs4020377](https://doi.org/10.3390/rs4020377).
- Wang, Y., J. Hyypä, X. Liang, H. Kaartinen, X. Yu, E. Lindberg, J. Holmgren, Y. Qin, C. Mallet, and A. Ferraz. 2016. "International Benchmarking of the Individual Tree Detection Methods for Modeling 3-D Canopy Structure for Silviculture and Forest Ecology Using Airborne Laser Scanning." *IEEE Transactions on Geoscience and Remote Sensing* 54 (9): 5011–5027. doi:[10.1109/TGRS.2016.2543225](https://doi.org/10.1109/TGRS.2016.2543225).
- Wolf, B.-M. and C. Heipke. 2007. "Automatic Extraction and Delineation of Single Trees from Remote Sensing Data." *Machine Vision and Applications* 18 (5): 317–330. doi:[10.1007/s00138-006-0064-9](https://doi.org/10.1007/s00138-006-0064-9).
- Wu, B., B. Yu, W. Yue, S. Shu, W. Tan, C. Chunling, Y. Huang, J. Wu, and H. Liu. 2013. "A Voxel-Based Method for Automated Identification and Morphological Parameters Estimation of Individual Street Trees from Mobile Laser Scanning Data." *Remote Sensing* 5 (2): 584–611. doi:[10.3390/rs5020584](https://doi.org/10.3390/rs5020584).
- Yao, W., J. Krull, P. Krzystek, and M. Heurich. 2014. "Sensitivity Analysis of 3D Individual Tree Detection from LiDAR Point Clouds of Temperate Forests." *Forests* 5 (6): 1122–1142. doi:[10.3390/f5061122](https://doi.org/10.3390/f5061122).